

COMPARISON OF THE CORROSION BEHAVIOR AND SURFACE MORPHOLOGY OF NiTi ALLOY AND STAINLESS STEELS IN SODIUM CHLORIDE SOLUTION

S. Kožuh*^a, L. Vrsalović^b, M. Gojić^a, S. Gudić^b, B. Kosec^c

^a University of Zagreb, Faculty of Metallurgy, Sisak, Croatia

^b University of Split, Faculty of Chemistry and Technology, Split, Croatia

^c University of Ljubljana, Faculty of Natural Sciences and Engineering, Ljubljana, Slovenia

(Received 29 January 2015; accepted 29 June 2015)

Abstract

The corrosion behavior of NiTi alloy and stainless steels (AISI 316L and X2CrNiMoN22-5-3) in 0.9% sodium chloride (0.154 mol⁻¹) solution was investigated using open circuit potential measurements, potentiodynamic polarization and electrochemical impedance spectroscopy measurements. Microstructural analyses before and after electrochemical tests were performed with the scanning electron microscopy (SEM) equipped with energy dispersive spectrometry (EDS). The lowest corrosion current density has NiTi alloy and the extent of the passive range increased in the order AISI 316L stainless steel < NiTi alloy < X2CrNiMoN22-5-3 duplex stainless steel. The oxide film formed on all samples has a double-layer structure consisting of a barrier-type inner layer and a porous outer layer. Oxide films formed on the surface of steels mainly contains iron oxides and chromium oxide, while the surface film of the NiTi alloy mainly contains TiO₂ oxide.

Key words: NiTi alloy; Stainless steel; EIS; SEM; Corrosion; Passive films

1. Introduction

Biomedical materials play an important role in the manufacturing of a variety of prosthetic devices in the modern world. Among them, metallic materials are being increasingly used in medical applications as implants to restore lost functions or to replace organs functioning below acceptable levels. The first requirement for any material to be placed in human body is its biocompatibility, i.e. the used material should not cause any adverse biological reaction in the body and it must be stable and have the ability to retain its functional properties.

It is known that NiTi alloys, like CuAlNi alloys, belong to the group of shape memory alloys [1,2]. However, while CuAlNi alloys have good corrosion resistance, they do not have good biocompatibility like that of NiTi alloy [3]. Therefore, the common materials that are currently used for implants include stainless steels and titanium alloys. Nickel-titanium alloys (Nitinol) possess unique thermal shape memory and superelasticity effects as well as good corrosion resistance, which makes these alloys very attractive for orthodontic and orthopaedics medical use. With its optimal combination of mechanical and excellent corrosion resistance and good biocompatibility, more than 1000 tons of devices made from titanium alloys

are implanted in patients worldwide every year [4]. Austenitic stainless steel of type AISI 316L is known as the most commonly used orthopaedic and orthodontic bracket materials because of its excellent mechanical properties such as high tensile strength and relatively high corrosion resistance in various aqueous environments. However its lower resistance of localized corrosion led to its replacement with duplex stainless steel [5]. The combination of two phases, delta – ferrite and austenite phases in the metallurgical structure of duplex steel and higher content of Cr in combination with Mo and Ni gives this material its unique mechanical properties and improved corrosion resistance in chloride media.

Corrosion of metal implants is critical because it can adversely affect the biocompatibility and mechanical integrity of the implant [4,6]. The environment in the human body is a buffered saline solution with pH around 7.4 and a temperature of 37 °C, which represents an excellent electrolyte and facilitates the electrochemical mechanisms of corrosion and hydrolysis. The corrosion resistance of NiTi and steel alloys depends on the passive film, which spontaneously forms (passivation) and reforms (repassivation) in the air and under most fluid conditions. Thus, the high corrosion resistance of NiTi alloy results from the formation of very stable,

* Corresponding author: kozuh@simet.hr

continuous adherent and protective oxide film on its surface which consists mainly of TiO₂ based oxides [7-9]. However, the oxides formed on the NiTi alloy surface always contain a certain fraction of Ni which could be released if corrosion processes take place [8,9]. It is clear that the nickel released from implant services in the human body is not desirable. The corrosion resistance of austenitic and duplex steels is owed to the presence of thin oxide film composed of Cr-oxide and Fe-oxide sub layers. However, the passive/protective nature of the passive film is generally attributed to the presence of Cr-oxide [10, 11]. Although the resistance of stainless steel passive films to general corrosion is relatively high, the films are susceptible to localized forms of corrosion. The potential hazard, associated with corrosion in the use of Ni and/or Cr containing alloys, comes from the biological and cytotoxic side effects of released Ni and Cr ions [12-17]. Nickel and chromium induce a type-IV hypersensitivity reaction in body, act as a hapten, carcinogen and mutagen. These metals cause several cytotoxic responses including a decrease in some enzyme activities, interference with biochemical pathways, carcinogenicity and mutagenicity [18-20].

In the present investigation, a systematic study was carried out in order to understand and compare the stability of different materials which have the potential for bio-medical application in 0.9 % sodium chloride solution (physiological saline solution) at pH = 7.4 and T = 37 °C. This solution is specified as the electrolyte in ASTM Standard F746 for corrosion testing metallic surgical implant materials [21]. Another aim of the paper is to compare the corrosion characteristics of NiTi alloy, AISI 316L austenitic stainless steel and X2CrNiMoN22-5-3 duplex stainless steel and surface morphology after exposure to 0.9% sodium chloride solution.

2. Experimental

The NiTi alloy (Table 1) was casted in a vacuum induction furnace in ingot with 45×45×110 mm dimensions. The ingot was annealed at 1000 °C followed by cooling in water. Subsequently, the ingot was heated to 850 °C and hot forged into bars with a different diameter (26 and 12 mm, respectively). The hot rolling into bars with diameter 8 and 6 mm followed after that. Prepared samples with a diameter of 4 mm were used for microstructural and corrosion investigations. A hot rolled plate measuring 500×200 mm with 15 mm thickness, made from AISI 316L austenitic stainless steel (Table 1) was used for investigation. From the plate a sample for microstructure and corrosion properties testing was cut. Also, a 16 mm thick hot rolled plate (300×300 mm) made from X2CrNiMoN22-5-3 duplex stainless steel (Table 1) was used for the preparation of samples in this investigation.

Table 1. The composition of the NiTi alloy, AISI 316L austenitic stainless steel and X2CrNiMoN22-5-3 duplex stainless steel, wt. %

Material	Chemical Composition, wt. %
NiTi alloy	49.16% Ti, 49.75% Ni
AISI 316L austenitic stainless steel	16.64 % Cr, 10.68 % Ni, 2.53 % Mo, 0.47 % Si, 0.002% C, 0.024% Nb, 0.009% S, 0.0045 % P, 69.60 % Fe
X2CrNiMoN22-5-3 duplex stainless steel	22.21% Cr, 5.47% Ni, 3.14% Mo, 1.52% Mn, 0.33% Si, 0.26 % Cu, 0.012 % C, 0.035 % V, 0.012 % Nb, 67.00 %Fe

The electrical contact for the electrochemical measurements was achieved by soldering the samples with the copper wire and then isolated with polyester leaving only one side to be exposed to the electrolyte. The electrode surface area prepared for exposure to the electrolyte was 0.125 cm² for NiTi alloy, 0.4 cm² for X2CrNiMoN22-5-3 duplex stainless steel and 1.92 cm² for AISI 316L steel. Prior to each measurement the electrode surface was ground successively with different grades of SiC paper down to 1000 grit. After that, the samples were ultrasonically cleaned in ethanol and deionized water. The corrosion resistance of the investigated materials was tested by using different electrochemical techniques in 0.9 % NaCl solution (0.154 mol⁻¹) pH = 7.4 which simulated the body fluid environment, at 37 °C.

A standard three-electrode cell, with Pt-plate counter electrode and saturated calomel electrode as the reference electrode, was used. The total amount of the electrolyte taken in the cell was 150 ml. All electrochemical measurements were performed with a PAR 273A potentiostat/galvanostat and a PAR M5210 lock-in amplifier for EIS measurements.

An open circuit potential of the sample was continuously monitored for 20 hours, and the potential was recorded as a function of time every 30 s. Potentiodynamic polarization measurements were performed in the potential range from -0.6 to 1.0 V with a scanning rate of 0.3 mV/s. The electrode was immersed in the test solution for 60 minutes prior to the potentiodynamic polarization measurements. Electrochemical impedance spectroscopy tests were carried out at E_{oc} using the signal amplitude of 10 mV and a frequency interval from 0.01 Hz to 50 kHz. EIS measurements were performed after 1, 3, 6, 12 and 24 hours.

The surface morphology of the samples before and after the potentiodynamic and EIS measurements was examined by scanning electron microscopy (SEM) equipped with energy dispersive spectrometer (EDS). Samples of steels for microstructural analyses before electrochemical testing were subsequently ground,

polished and etched in solution 5g copper (II) chloride + 100 ml hydrochloric acid + 100 ml ethanol, while a sample of NiTi alloy was investigated in non etched state.

3. Results and discussion

SEM microstructure analysis of investigated materials was performed before electrochemical investigations. The results of analysis of the microstructure are shown on Fig. 1. The microstructure of AISI 316L steel is shown in Fig. 1a. Microstructure of AISI 316L steel is primarily a single phase structure (austenite) with a few fields of ferrite. In the ideal case, austenitic stainless steels contain a single phase that is stable over a wide temperature range. However, such a microstructure is more sensitive to cracking than one containing a small amount of ferrite. Therefore, AISI 316L steel showed polygonal grains of austenite with a low delta ferrite content. Also, SEM analysis showed that the duplex stainless steel of grade X2CrNiMoN22-5-3, consisted of austenite and ferrite in roughly equal proportions (Fig. 1b). Both the austenite and ferrite were elongated in the direction of rolling. It can be seen in Fig. 1c that surface morphology of NiTi alloy is smooth with small inclusions which are visible in the matrix alloy.

The open circuit potentials (E_{OC}) reflect the composite results of the electrochemical reactions which take place at the electrode and solution interface. Therefore, monitoring the changes of open circuit potential with immersion time can be employed to study the electrochemical processes. Fig. 2 displays the E_{OC} of NiTi alloy, AISI 316L austenitic stainless steel and X2CrNiMoN22-5-3 duplex stainless steel specimens as a function of immersion time in a 0.9% sodium chloride solution.

From Fig. 2 it can be seen that the open circuit

potential of NiTi alloy in 0.9 % sodium chloride solution increases gradually towards a nobler direction during the immersion. The initial value of E_{OC} of the NiTi alloy was -0.236 V(SCE) and it changed to the positive direction rapidly in the first 20 minutes. After that point the potential values changed slowly to the positive values and after 1200 minutes reached the value of -0.154 V(SCE). This change in E_{OC} value was probably due to the formation and thickening of the protective oxide film on the NiTi alloy surface which, according to the literature, consists of mainly titanium oxides [22].

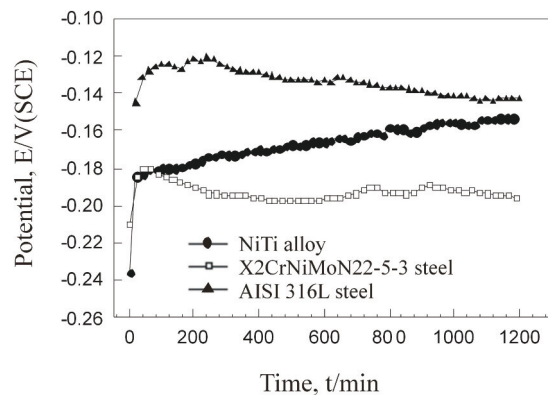


Figure 2. Variation of the open circuit potentials of AISI 316L austenitic stainless steel, X2CrNiMoN22-5-3 duplex stainless steel and NiTi alloy in 0.9 % sodium chloride solution

The changes of E_{OC} vs. time for the X2CrNiMoN22-5-3 duplex stainless steel in 0.9 % sodium chloride solution showed an initial positive shift of about 40 mV(SCE) to the value of approximately -0.18 V(SCE), followed by small potential decrease, approximately 10 mV, and after that potential stabilisation around -0.185 V. This

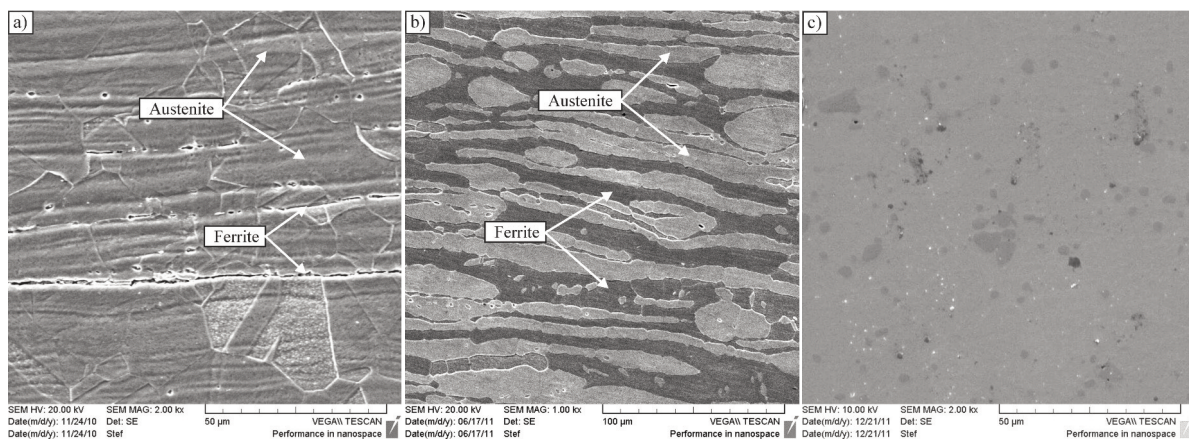


Figure 1. SEM micrographs of AISI 316L austenitic stainless steel (a), X2CrNiMoN22-5-3 duplex stainless steel (b) and NiTi alloy (c) before electrochemical testing

positive potential shift is probably due to build up of the thicker passive surface layer due to the presence of dissolved oxygen in the sodium chloride solution. Similar behavior was seen within the AISI 316L steel. In the first 75 minutes the potential changed towards the positive direction and after that stabilized at the highest positive value in comparison with the other two materials investigated.

Potentiodynamic polarization testing was conducted on the investigated metals (NiTi alloy, AISI 316L austenitic stainless steel and X2CrNiMoN22-5-3 duplex stainless steel) to determine their individual corrosion behavior under static conditions in 0.9% sodium chloride solution. The results of this investigation were presented in Fig. 3, which shows the potentiodynamic polarization curves obtained in sodium chloride solution for the three types of materials examined.

For the X2CrNiMoN22-5-3 duplex stainless steel the presence of wide passivation plateau was observed, while for the NiTi alloy and AISI 316L austenitic stainless steel passivity occurred in a shorter range of potentials, indicating a higher tendency towards localized corrosion. The electrochemical parameters from the polarization curves are presented in Table 2.

From Fig. 3 and Table 2 it can be seen that AISI 316L austenitic stainless steel have the highest

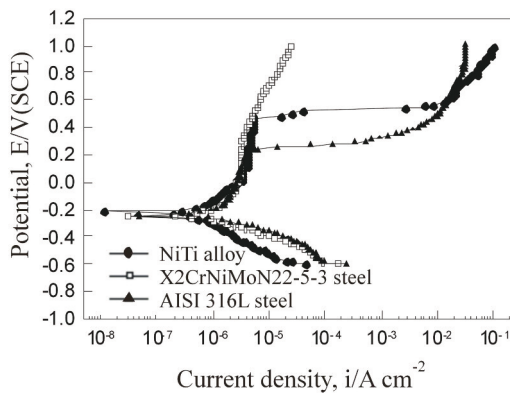


Figure 3. Potentiodynamic curves of AISI 316L austenitic stainless steel, X2CrNiMoN22-5-3 duplex stainless steel and NiTi alloy in 0.9 % sodium chloride solution

corrosion current and the lowest breakdown potential which indicates its lowest resistance for the localized corrosion attack. The passive range is established in potential range approximately from -0.185 V(SCE) to 0.240 V(SCE) (0.425 V). The value for breakdown potential of AISI 316L austenitic stainless steel is in accordance with literature data for the investigations in similar conditions [6, 23, 24].

The polarization curve of the NiTi alloy is characterized by a passive region extending from about -0.001 V(SCE) to 0.480 V(SCE) (0.481 V). Although the corrosion current has the lowest value, which suggests the high corrosion resistance of NiTi alloy, the passive region is relatively small which indicates the susceptibility for localized corrosion. This was supported with already established findings: first, the potential value of 800 mV was established as a threshold for immunity to localized corrosion, and second, the highest potential values that titanium and its alloys can attain in vivo conditions was in the range of 450-550 mV versus SCE [25]. The pitting potential was below given potential limits which indicated the possibility of localized corrosion attack. The pitting potential of duplex stainless steel is higher than other investigated material and cannot be determined from its polarization curve. If we use another criterion for determining the pitting potential, when the pitting potential is the value of potential corresponding to anodic current density of $10 \mu\text{A}/\text{cm}^2$ [25], then the value of pitting potential of duplex stainless steel would be around 710 mV. The value of the corrosion current is somewhat higher than the corrosion current of NiTi alloy but much smaller than AISI 316L austenitic stainless steel, which indicates the possibility of a potential application of X2CrNiMoN22-5-3 duplex stainless steel in medicinal use.

The corrosion rate, for investigated alloys, was calculated by using the equation:

$$v_{\text{corr}} = \frac{i_{\text{corr}} \times M}{d \times F \times z} \quad (1)$$

where i_{corr} is the corrosion current density in Acm^{-2} , M is the molar mass of the corroded species in $\text{g}\cdot\text{mol}^{-1}$, d is density of corroding species in $\text{g}\cdot\text{cm}^{-3}$, F is the Faraday constant, $96487 \text{ C}\cdot\text{mol}^{-1}$ and z is the electron number. From the Table 2 it can be seen that the

Table 2. The electrochemical parameters obtained from potentiodynamic polarization measurements for NiTi alloy, AISI 316L austenitic stainless steel and X2CrNiMoN22-5-3 duplex stainless steel in 0.9 % sodium chloride solution

Material	$i_{\text{corr}} / \mu\text{A cm}^{-2}$	$E_{\text{corr}} / \text{V}$	$b_c / \text{V dec}^{-1}$	$b_a / \text{V dec}^{-1}$	E_b / V	$v_{\text{corr}} / \text{mm a}^{-1}$
NiTi alloy	0.42	-0.224	-0.2508	0.2934	≈ 0.470	0.00364
AISI 316L austenitic stainless steel	1.05	-0.234	-0.1309	0.2336	≈ 0.245	0.0109
X2CrNiMoN22-5-3 duplex stainless steel	0.68	-0.24	-0.127	0.189	-	0.00719

lowest corrosion rate has NiTi alloy, the highest corrosion rate has AISI 316L austenitic stainless steel while the value of the corrosion rate of X2CrNiMoN22-5-3 duplex stainless steel is falling between the values for these two alloys. This is in accordance with the surface morphology obtained after potentiodynamic measurements. As can be seen, the surface of AISI 316L austenitic stainless steel is significantly damaged by corrosion, while surface damages of X2CrNiMoN22-5-3 duplex stainless steel are considerably less (Fig. 4a and 4b). The breakdown of passive film on the NiTi alloy surface is clearly visible on Fig. 4c.

The open circuit impedances of the NiTi alloy, AISI 316L austenitic stainless steel and X2CrNiMoN22-5-3 duplex stainless steel were traced over 24 hours from the electrode immersion into 0.9% sodium chloride solution at 37 °C, and some the obtained results are presented in Figs. 5 and 6. Impedance measurements were made on investigated alloys at time intervals of 1, 3, 6, 12 and 24 hours after immersion of the electrode into the electrolyte. The shape of the impedance curves was the same for the measuring time interval, with the different values of parameters of equivalent circuit.

The Nyquist diagrams of all samples determined after different immersion times show fragments of a large incomplete semicircle, which represent the typical impedance response for tin oxide films.

In Bode plots at high frequencies ($f > 1$ kHz), the impedance is almost independent of the frequency with the phase angle approaching 0°. This is the representative response reflecting a resistive behaviour and corresponds to electrolyte resistance. At medium and low frequencies the capacitive behaviour of examined systems is evident. A Bode slope of ≈ -1 and phase angles approaching -90° are characteristic for this frequency range, suggesting that a highly stable oxide film was formed on all tested

materials. Furthermore, for all tested materials the module of impedance increases with time in order AISI 316L austenitic stainless steel < X2CrNiMoN22-5-3 duplex stainless steel < NiTi alloy. This is consistent with the low corrosion current obtained from polarization measurements.

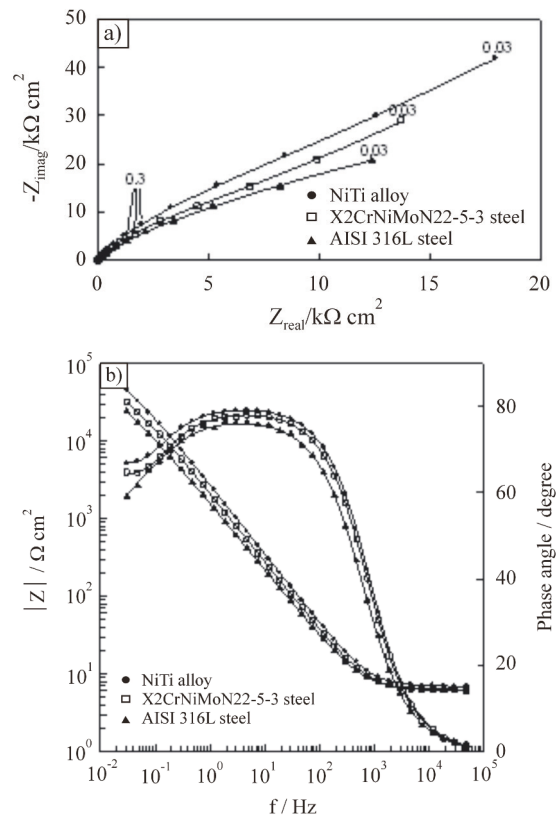


Figure 5. Nyquist (a) and Bode (b) plots recorded on NiTi alloy, AISI 316L austenitic stainless steel and X2CrNiMoN22-5-3 duplex stainless steel after 1 hour of immersion in 0.9% sodium chloride solution

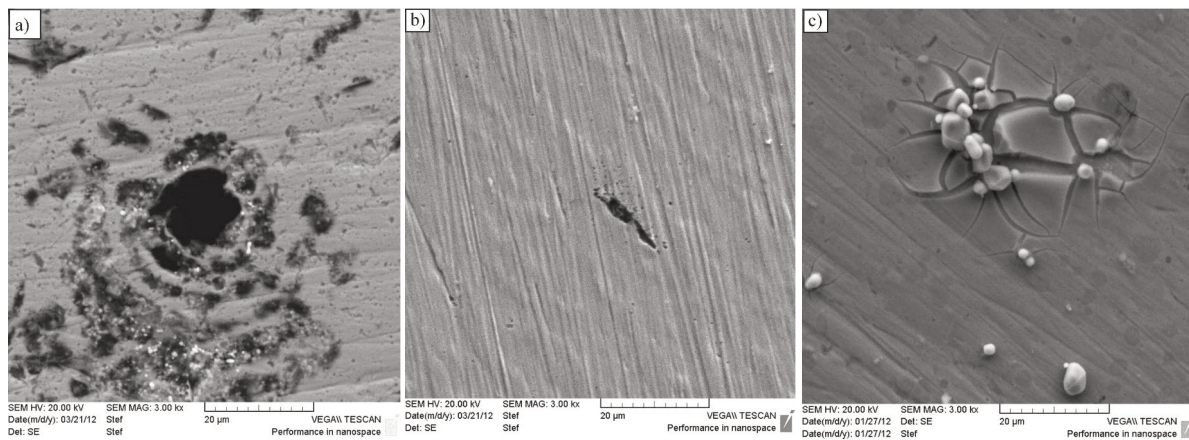


Figure 4. SEM micrographs of AISI 316L austenitic stainless steel (a), X2CrNiMoN22-5-3 duplex stainless steel (b) and NiTi alloy (c) after potentiodynamic polarization measurements in 0.9% sodium chloride solution

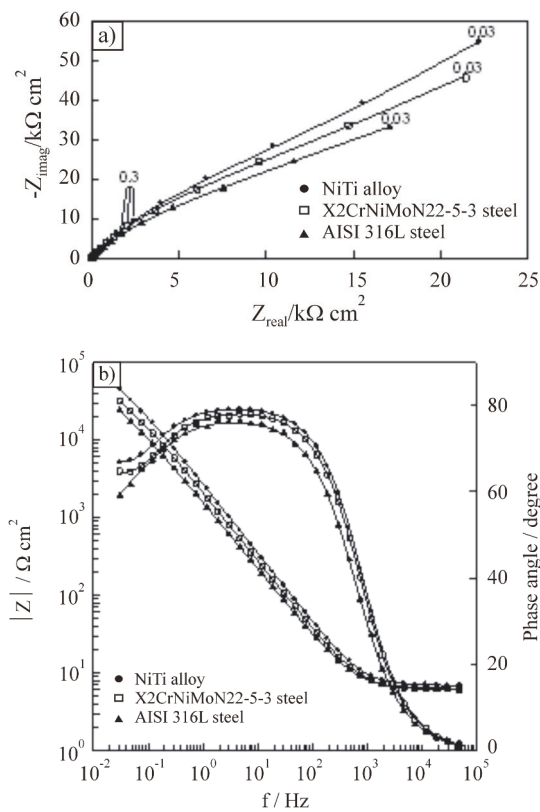


Figure 6. Nyquist (a) and Bode (b) plots recorded on NiTi alloy, AISI 316L austenitic stainless steel and X2CrNiMoN22-5-3 duplex stainless steel after 24 hours immersion in 0.9% sodium chloride solution

The large phase angle peak could be indicative of the interaction of at least two time constants. Hence, the EIS results can be best described by the equivalent circuit shown in Fig. 7. It consists of the electrolyte resistance, R_{el} ($\approx 6 \text{ W cm}^2$), connected in series with two parallel time constants. This equivalent circuit is based on a model used by Pan et al. [26] to simulate data for titanium in the saline solution, and can be regarded as an electrical representation of a two-layer model of oxide film, consisting of a barrier-like inner layer and a porous outer layer. This model is often used in the literature to represent the oxide film on NiTi alloy and other Ti implant alloys [27-29]. A two-layer structure has also been hypothesized for the passive film on stainless steels [30, 31]. In this model, R_p corresponds to the porous layer resistance, R_b to the barrier layer resistance, Q_p to the constant phase element of the outer porous layer and Q_b to the constant phase element of the inner barrier layer.

The constant phase elements (CPEs) replaced the capacitive elements in the proposed equivalent circuit. In many cases the CPE was introduced formally only for fitting the impedance data to account for deviations observed as the capacitive loop is

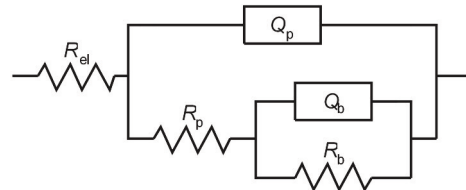


Figure 7. Proposed equivalent circuit used for fitting impedance data

depressed. Its impedance, Z_{CPE} , is described by the expression $Z_{CPE} = [Q(j\omega)^n]^{-1}$ with $-1 \leq n \leq 1$, $j = (-1)^{1/2}$ and $\omega = 2\pi f$ [32]. The Q is a frequency independent constant, being defined as pure capacitance for $n = 1$, resistance for $n = 0$, inductance for $n = -1$. Diffusion processes are characterized by the value of $n = 0.5$. According to the fitting results, the n values for Q_p are about 0.88, while the n values for Q_b are close to 0.92. This shows that Q_p and Q_b contains some frequency dispersion. The evolutions of the fitted parameters with immersion time for all examined samples are presented in Table 3.

It can be seen that the resistance of the inner barrier layer, R_b , of NiTi alloy is $\approx 400 \text{ kW cm}^2$ during the early stages of immersion, increasing up to values of $\approx 700 \text{ kW cm}^2$, after which it stayed more-or-less constant. The increase of R_b may be attributed to a regrowth of the inner layer or to a self-healing process. These processes are known to occur in passive film on titanium and imply that the film become more corrosion protective [26]. In addition, the capacity of barrier layer Q_b , decreases slightly with exposure time, demonstrating that the passive film increases and then tends to become stable. The slight decrease of Q_b may correspond to a slow growth of the surface oxide film which is mainly consisting of TiO_2 [22].

Furthermore, as shown in Table 3, R_p increases with exposure time, while the corresponding capacity, Q_p , decreases slightly with continued immersion.

It is worth noting that R_b was higher than R_p by a factor of 6-7, showing that the resistance of the oxide film on the NiTi alloy is due to the barrier layer. On the other hand, the Q_b and Q_p have similar values at all immersion times. It is believed that the outer porous layer consists of the same oxide as the inner barrier layer but with microscopic pores. It is also generally agreed that the pores in the outer layer may be filled with electrolytes, and this might have contributed to the larger values of Q_p comparatively to Q_b .

Namely, the porous film dielectric constant depends on the dielectric constant of the solution and on the pore number and size due to the existence of solution inside the pores. The value of the film dielectric constant increases with the film porosity that is with the solution quantity inside the film, because the solution dielectric constant is higher than

Table 3. Parameters of equivalent circuit for NiTi alloy, X2CrNiMoN22-5-3 duplex stainless steel and AISI 316L austenitic stainless steel in 0.9% sodium chloride solution after EIS measurements

Material	Time / h	$Q_p \times 10^6 / \Omega^{-1} s^n cm^{-2}$	n_1	$R_p / k\Omega cm^2$	$Q_b \times 10^6 / \Omega^{-1} s^n cm^{-2}$	n_b	$R_b / k\Omega cm^2$
NiTi alloy	1	71.48	0.89	82.57	50.52	0.91	414.83
	3	65.4	0.88	91.48	44.68	0.91	552.31
	6	62.35	0.89	98.48	40.82	0.92	646.47
	12	60.65	0.88	108.88	39.4	0.92	728.2
	24	56.78	0.89	120	37.56	0.92	704.12
X2CrNiMoN22-5-3 duplex SS ^[a]	1	93.98	0.88	50.68	78.74	0.9	272.9
	3	76.22	0.88	61.29	56.81	0.91	349.35
	6	67.39	0.88	65.44	58.62	0.91	403.22
	12	67.53	0.87	76.59	53.53	0.91	442.44
	24	64.38	0.89	97.28	52.06	0.89	476.79
AISI 316L austenitic SS ^[a]	1	130.78	0.86	40.49	110.87	0.89	55.65
	3	104.31	0.86	48.8	95.51	0.9	102.51
	6	96.34	0.87	54.44	91.94	0.91	117.65
	12	94.54	0.87	65.74	85.32	0.9	147.65
	24	88.39	0.87	80.41	80.48	0.9	185.07

^[a] SS – stainless steel

the titanium oxide dielectric constant.

Table 3 also shows the circuit parameters for AISI 316L austenitic stainless steel and X2CrNiMoN22-5-3 duplex stainless steels as a function of immersion time. These data are similar to the data already presented for the NiTi alloy. Again, the values of R_b and R_p increase with exposure time, while the Q_b and Q_p decrease. Corrosion resistance of these alloys is also ascribed to the barrier layer, which is mainly consisting of chromium and iron oxides [33]. Namely, the R_b was higher than R_p by a factor of 5-6 for duplex stainless steel, and by factor of 2-3 for AISI 316L stainless steel, while the Q_b and Q_p of both types of steel have similar values.

The capacitance of barrier film ($n \approx 0.92$; $Q_b \approx C$) can be used to estimate the passive film thickness, based on equation $C = \epsilon_0 \epsilon / d$, which is valid for the parallel plate capacitor model of the homogenous oxide layer. In this equation ϵ_0 is the permittivity of the free space ($\epsilon_0 = 8.85 \cdot 10^{-12} \text{ F m}^{-1}$), and ϵ is the dielectric constant of the passive film. However, it should be noted that it is difficult to obtain an accurate thickness value of the passive film when the dielectric constant is not well established. Particular uncertainty exists in the case of determining the dielectric constant of the passive film on the steel samples, since the surface film consist of the mixed type oxide film, as it confirmed in the EDS analysis. The proposed values for dielectric constant in the literature are from 10 to 40

[31, 33-35]. The EDS analysis (Figs. 8b and 9b) showed oxygen concentration on the top surface, which reflects on the oxides presence on the surface. For AISI 316L austenitic stainless steel the contamination with carbon and silicon is observed. The primary constituents of the passive layer of AISI 316L austenitic stainless steel are chromium and ferrous oxides while the content of molybdenum and nickel oxides is probably very low (Fig. 8b). Unlike steel, the EDS analysis shows that the surface oxide film on NiTi alloy is mainly consisting of TiO_2 (Fig. 9), whose dielectric constant values are in the range of 80-100 [27, 34]. Nevertheless, since the capacitance is inversely proportional to the layer thickness, the capacitive response of the alloys can give an indication of how the thickness of the passive film changes. In this sense, it can be observed that the constant phase element Q_b decreased in the following order: AISI 316L austenitic stainless steel > X2CrNiMoN22-5-3 duplex stainless steel > NiTi alloy, suggesting that the passive films thickness increases in the inverse order. The corrosion resistance of investigated alloys increases in the same direction.

While the corrosion resistance of tested alloys is attributed to the barrier layer, its ability to osseointegrate can be attributed to the presence of the porous layer. It seems reasonable to assume that as soon as the implantation is completed, the bone cell (osteoblast-like cells) tend to migrate inside the pores

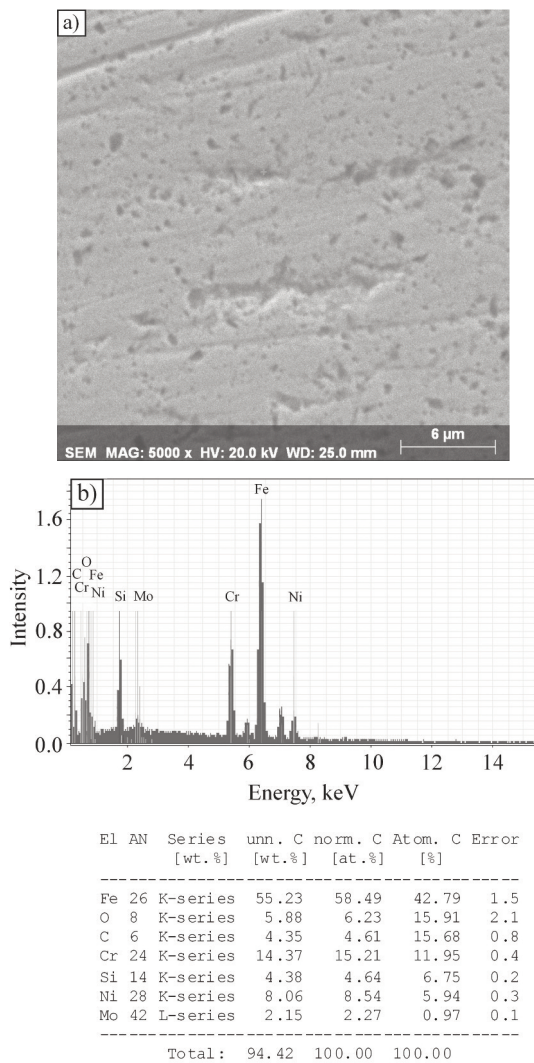


Figure 8. SEM micrograph of surface morphology (a) and EDX spectrum (b) of AISI 316L austenitic stainless steel after impedance measurements over a period of 24 hours immersion in 0.9% sodium chloride solution

of the passive film. This interpretation certainly facilitates the adhesion between the implant and the bone (implant anchorage). In this way, the osseointegration is not only accelerated but also more effective because of increasing non-uniform contact surface [29].

4. Conclusions

The corrosion behaviour of NiTi alloy, AISI 316L austenitic stainless steel and X2CrNiMoN22-5-3 duplex stainless steel in 0.9% sodium chloride solution was investigated using open circuit potential measurements, potentiodynamic polarization and electrochemical impedance spectroscopy

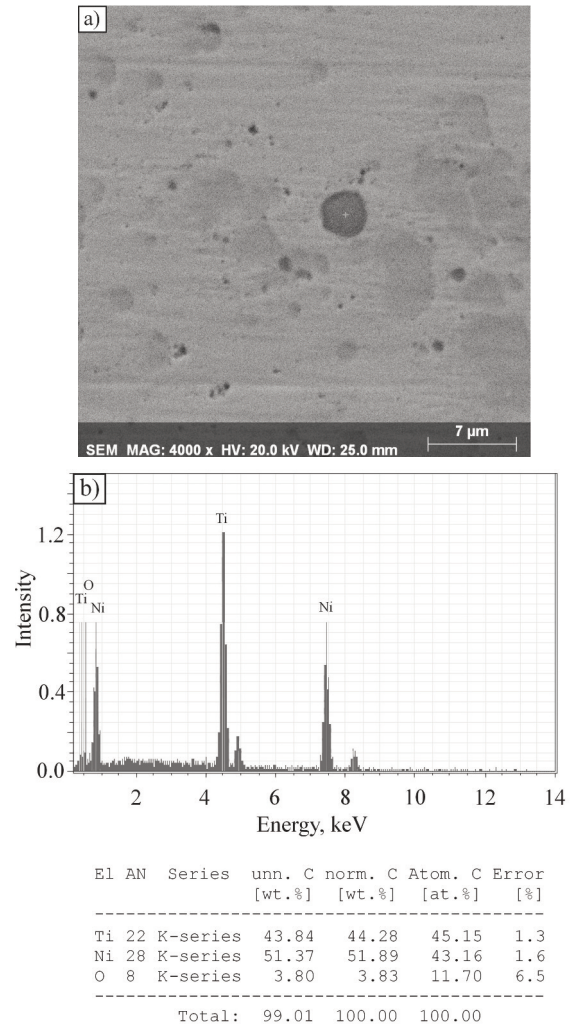


Figure 9. SEM micrograph of surface morphology (a) and EDX spectrum (b) of NiTi alloy after impedance measurements over a period of 24 hours immersion in 0.9% sodium chloride solution

measurements. The results of the electrochemical investigations and microstructure analysis by SEM suggest the following conclusions:

1. The results of open circuit potential measurements for all investigated alloys in 0.9% sodium chloride solution indicated the formation of protective passive oxide film on their surfaces.

2. Potentiodynamic polarization measurements have shown that the lowest corrosion current density and the lowest corrosion rate had NiTi alloy and the extent of the passive range increased in order AISI 316L austenitic stainless steel < NiTi alloy < X2CrNiMoN22-5-3 duplex stainless steel.

3. SEM images after potentiodynamic measurements revealed that the surface of AISI 316L austenitic stainless steel was significantly damaged by

corrosion, while surface damages of X2CrNiMoN22-5-3 duplex stainless steel, and NiTi alloy, were considerably less.

4. The impedance measurements at open circuit potential reveal that the oxide film formed on all samples has a double-layer structure, consisting of a barrier-type inner layer and a porous outer layer. The corrosion resistance of the tested alloys is ascribed to the barrier layer.

5. For all tested materials the module of impedance increased with time in order AISI 316L austenitic stainless steel < X2CrNiMoN22-5-3 duplex stainless steel < NiTi alloy due to continuous growth of the passive film on the alloy surface.

6. The EDS analysis showed that the surface oxide films found on the steels used were the mixed type oxide, mainly composed of iron oxides and chromium oxide, while the surface film on NiTi alloy mainly consisted of TiO₂ oxide.

References

- [1] R. Lahoz, J.A. Puértolas, *J. Alloy. Compd.*, 381 (2004) 130-136.
- [2] M. Gojić, L. Vrsalović, S. Kožuh, A.C. Kneissl, I. Anžel, S. Gudić, B. Kosec, M. Klišković, *J. Alloy. Compd.*, 509 (2011), 9782-9790.
- [3] A. Creuziger, W.C. Crone, *Acta Mater.*, 56 (2008) 518-526.
- [4] G. Manivasagam, D. Dhinasekaran, A. Rajamanickam, *Recent Patents on Corrosion Science*, 2 (2010) 40-54.
- [5] M. Conradi, P.M. Schon, A. Kocijan, M. Jenko, G.J. Vancso, *Mater. Chem. Phys.*, 130 (2011) 708-713.
- [6] I. Gurappa, *Mater. Charact.*, 49 (2002) 73-79.
- [7] L. Tan, R.A. Dodd, W.C. Crone, *Biomaterials*, 24 (2003) 3931-3939.
- [8] S.A. Shabalovskaya, G.C. Rondelli, A.L. Undisz, J.W. Anderegg, T.D. Burleigh, M.E. Rettenmayr, *Biomaterials*, 30 (2009) 3662-3671.
- [9] S.A. Shabalovskaya, H. Tian, J.W. Anderegg, D.U. Schryvers, W.U. Carroll, J.V. Humbeeck, *Biomaterials*, 30 (2009) 468-477.
- [10] A. Shahryari, S. Omanović, J.A. Szpunar, *Mat. Sci. Eng. C.*, 28 C (2008) 94-106.
- [11] I. Juraga, V. Šimunović, Đ. Španiček, *METABK*, 46 (2007) 185-189.
- [12] H. Kerosuo, G. Moe, E. Kleven, *Angle Orthod.*, 2 (1995) 111-116.
- [13] B. Guyuron, C. Lasa, *Plast. Reconstr. Surg.*, 89 (1992) 540-542.
- [14] J. Ryhanen, E. Niemi, W. Serlo, E. Niemela, P. Sandvik, H. Pernu, T. Salo, *J. Biomed. Mat. Res.*, 35 (1997) 451-457.
- [15] H. Kim, J.W. Johnson, *Angle Orthod.*, 69 (1999) 39-44.
- [16] R. Koster, D. Vieluf, M. Kiehn, M. Sommerauer, J. Kahler, S. Baldus, T. Meinertz, C.W. Hamm, *Lancet*, 356 (2000) 1895-1897.
- [17] M. Geetha, A.K. Singh, R. Asokamani, A.K. Gogia, *Prog. Mater. Sci.*, 54 (2009) 397-425.
- [18] M.L. Pereira, A. Silva, R. Tracana, G.S. Carvalho, *Cytobios*, 77 (1994) 73-80.
- [19] N.K. Veien, E. Bochhorst, T. Hattel, G. Laurberg, *Contact Dermatitis*, 30 (1994) 210-213.
- [20] T.P. Chaturvedi, http://orthocj.com/journal/uploads/2008/01/0054_en.pdf.
- [21] ASTM Standard F746-87. Standard test method for pitting and crevice corrosion of metallic surgical implant materials, West Conshohocken, PA: ASTM International; 1987 (Reproved 1999).
- [22] T. Hu, C.L. Chu, Y.C. Xin, S.L. Wu, K.W.K. Yeung, P.K. Chu, *J. Mater. Res.*, 25 (2) (2010) 350-358.
- [23] K.Y. Chiu, F.T. Cheng, H.C. Man, *Surf. Coat. Tech.*, 200 (2006) 6054-6061.
- [24] K. Endo, M. Suzuki, H. Ohno, *Dent. Mater. J.*, 19 (2000) 34-49.
- [25] G. Rondelli, B. Vicentini, *Biomaterials*, 23 (2002) 639-644.
- [26] J. Pan, D. Thierry, C. Leygraf, *Electrochim. Acta*, 41 (1996) 1143-1153.
- [27] N. Figueira, T.M. Silva, M.J. Carmezim, J.C.S. Fernandes, *Electrochim. Acta*, 54 (2009) 921-926.
- [28] R. Venugopalan, J.J. Weimer, M.A. George, L.C. Lucas, *Biomaterials*, 21 (2000) 1669-1677.
- [29] I.C. Lavos-Valereto, S. Wolyneć, I. Ramires, A.C. Guastaldi, I. Costa, *J. Mater. Sci.-Mater. Med.*, 15 (2004) 55-59.
- [30] C.R. Clayton, I. Olefjord, *Passivity of austenitic stainless steels*, in: P. Marcus, J. Oudar, (Eds.), *Corrosion Mechanism Theory and Practice*, Marcel Dekker, New York, 1995, p. 175-199.
- [31] C.A. Della Rovere, J.H. Alano, R. Silva, P.A.P. Nascente, J. Otubo, S.E. Kuri, *Corr. Sci.*, 57 (2012) 154-161.
- [32] I.D. Raistrick, D.R. Franceschetti, J.R. Macdonald, *Theory*, in: E. Barsoukov, J.R. Macdonald (Eds.), *Impedance Spectroscopy*, second ed., J. Wiley & Sons, Inc., New Jersey, 2005.
- [33] D. Wallinder, J. Pan, C. Leygraf, A. Delblanc-Bauer, *Corr. Sci.*, 41 (1999) 275-289.
- [34] V. L'Hostis, C. Dagbert, D. Feron, *Electrochim. Acta*, 48 (2003) 1451-1458.
- [35] A. Kocijan, D. Kek Merl, M. Jenko, *Corr. Sci.*, 53 (2011) 776-783.